1998 International Computer Symposium
Workshop on Image Processing and Character Recognition
December 17-19, 1998, N.C.K.U., Tainan, Taiwan, R.O.C.

Advanced Combinations of Splitting-Shooting-Integrating Methods for Digital Image Transformations

Zi-Cai Li
Department of Applied Mathematics
National Sun Yat-sen University,Kaohsiung,Taiwan
E-mail:zcli@math.nsysu.edu.tw, Tel: (07)5252000, ext.3824; Fax:(07)5253824

November 2, 1998

Abstract

The greyness values at a pixel can also be represented by an integral as the mean of continuous greyness functions over a small pixel region. Based on such an idea, the discrete images can be produced by numerical integration; several efficient algorithms are developed to convert images under transformations. Among these algorithms, the combination of splitting-shooting-integrating methods (CSIM) is most promising because no solutions of nonlinear equations are required for the inverse transformation. The CSIM is proposed in [5] to facilitate images and patterns under a cycle transformations $T^{-1}T$, where T is a nonlinear transformation. When a pixel region in two dimensions is split into N^2 subpixels, convergence rates of pixel greyness by CSIM are proven in [7] to be only $O(1/N)$. In [8], the convergence rates $O_p(1/N^{1.5})$ in probability and $O_p(1/N^2)$ in probability using a local partition are discovered. In this paper, a partition technique for numerical integration is proposed to evaluate carefully any overlaps between the transformed subpixel regions and the standard square pixel regions. This technique is employed to evolve the CSIM such that the convergence rate $O(1/N^2)$ of greyness solutions can be achieved. The computational figures for real images of 256 x 256 with 256 greyness levels display that $N = 4$ is good enough for real applications. This clearly shows validity and effectiveness of the new algorithms in this paper.
Keywords: Numerical integration, digital images, image transformation, pattern recognition

1 Introduction

Usually, the approaches studying the discrete and continuous topics are quite different due to different natures, such as those in discrete and analytic mathematics. This paper demonstrates an example how to study discrete images by integrals and their numerical approximation. The key idea is as follows. Based on such an idea, the discrete images can be produced by numerical techniques. However, It is due to special nature of the integration from images transformations that renovation of the existing integration rules is necessary. Consequently, new discrete algorithms have been developed. In our past research on image transformation in [5] - [9], the study on discrete algorithms is, indeed, the study of numerical integration for the integrand without uniform smoothness. This paper also reveals how to employ numerical methods and error analysis to discrete topics effectively. Note that our research process looks pass a long, cycle road: from the discrete to the continuous, and then from the continuous back to the discrete, our destination. But a number of amazing results have been found, see [5] - [9]; one of them is reported in this paper. Several combined methods are proposed in [5] to facilitate restoration of digital images and patterns under T^{-1} T, where T is a nonlinear transformation defined by

$$\mathrm{T} : (\xi, \eta) \rightarrow (x, y), \; x = x(\xi, \eta) \;\; y = y(\xi, \eta), \quad (1.1)$$

and xoy and $\xi o \eta$ are two Cartesian coordinate systems. To bypass solving nonlinear equations, the combination CSIM is proposed in [5], in which we employ the splitting-shooting method for T given and the splitting-integrating method for T^{-1} given. An error analysis is made in [7] for estimating consecutive errors of pixel greyness solutions, to show that only a low convergence rate $O(1/N)$ can be obtained, where a pixel is split into N^2 subpixels.

The question asked here is: can we raise the convergence rates of pixel greyness solutions by CSIM? Paper [8] responds to this question. In [9], we employ probabilistic analysis, to discover that the convergence rates, $O_p(1/N^{1.5})$ in probability, can be obtained. Moreover, the high convergence rate, $O_p(1/N^2)$ in probability, can be achieved, if using a local partition. When $N \geq 32$

good figures of images are produced.

In this paper, the new technique is adopted in CSIM to lead to two new combinations $C\bar{S}IM$ and $C\bar{S}\bar{I}M$, where the notations '$\bar{S}$' and '$\bar{I}$' denote the renovated splitting-shooting method and the renovated splitting-integrating method, respectively. Both $C\bar{S}IM$ and $C\bar{S}\bar{I}M$ can grant the pixel image greyness under $T^{-1}T$ to have the convergence rate $O(1/N^2)$, based on strict error analysis without probability. The new combinations are simple and easy to carry out because no solutions of nonlinear equations are needed, either. Surprisingly, when the division number is chosen to be $N = 4$, good image pictures are produced.

Below, we describe and analyze the combination CSIM in Section 2, propose the new partition technique in Section 3, to lead to the new combinations $C\bar{S}IM$ and $C\bar{S}\bar{I}M$, then derive error bounds of transformed images by $C\bar{S}IM$ and $C\bar{S}\bar{I}M$ in Section 4, and finally in Section 5 provide numerical and graphical results to verify the convergence rate $O(1/N^2)$. Some real images of 256×256 pixels with 256 greyness levels display significance of the new algorithms in this paper.

2 Numerical Algorithms

Let a given standard image undergo a cycle conversion (see [5]).

$$\hat{W} \xrightarrow{T} \hat{Z} \xrightarrow{T^{-1}} \hat{W}, \ \hat{W} = \{\hat{W}_{ij}\} \ \hat{Z} = \{\hat{Z}_{IJ}\}, \quad (2.1)$$

where the pixels $\hat{W}_{ij}$ and $\hat{Z}_{IJ}$ are located at the points (i,j) and (I,J) respectively,

$$\begin{aligned}(i,j) &= \{(\xi,\eta) \ \ \xi = iH, \ \eta = jH\} \\ (I,J) &= \{(x,y), \ x = IH, \ y = JH\}, \end{aligned} \quad (2.2)$$

and H is the mesh resolution in an optical scanner. We will apply numerical approaches to perform (2.1), illustrated in Figure 1 with eight steps. In Steps 1 and 5, we convert image pixels and their greyness to each other. For the sake of simplicity, we assume the binary images, and choose

$$\Phi_{ij}, \ B_{ij} = \begin{cases} 1 & \text{if} \ \ W_{ij}, \ Z_{IJ} = \text{`*'}, \\ 0 & \text{if} \ \ W_{ij}, \ (Z_{IJ}) = \text{` '}, \end{cases} \quad (2.3)$$

Furthermore, if the values of greyness $\tilde{\Phi}_{ij}$ and $\tilde{B}_{IJ}$ have been obtained, in Steps 4 and 8 we may obtain image pixels by

$$\tilde{W}_{ij}, \ \tilde{Z}_{IJ} = \begin{cases} \text{`*'} & \text{when} \ \ \tilde{\Phi}_{ij}, \ \tilde{B}_{IJ} \geq \frac{1}{2}, \\ \text{`+'} & \text{when} \ \ \frac{1}{4} \leq \tilde{\Phi}_{ij}, \ \tilde{B}_{IJ} < \frac{1}{2}, \\ \text{`.'} & \text{when} \ \ 0.1 \leq \tilde{\Phi}_{ij}, \ \tilde{B}_{IJ} < \frac{1}{4}, \\ \text{` '} & \text{when} \ \ \tilde{\Phi}_{ij}, \ \tilde{B}_{IJ} < 0.1, \end{cases} \quad (2.4)$$

In Step 2, the following simplest piecewise constant and bilinear interpolatory functions are adopted. I. The

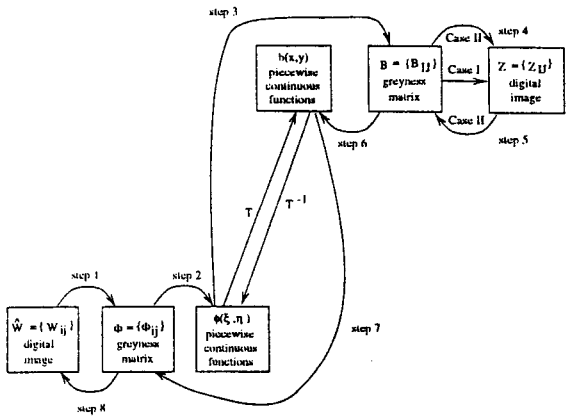

Figure 1: Schematic steps in digital images under transformations by numerical approaches

piecewise constant interpolation ($\mu = 0$)

$$\hat{\phi}_0(\xi,\eta) = \tilde{\Phi}_{ij} \ \text{ in } \square_{ij}, \ \ \textit{where} \quad (2.5)$$

$$\square_{ij} = \left\{ \begin{array}{ll} (\xi,\eta), & (i-\frac{1}{2})H \leq \xi < (i+\frac{1}{2})H, \\ & (j-\frac{1}{2})H \leq \eta < (j+\frac{1}{2})H \end{array} \right\}, \quad (2.6)$$

and the total domain Ω of the standard image $\hat{W}$ in $\xi o \eta$ is $\Omega = \bigcup_{ij} \square_{ij}$. II. The piecewise bilinear interpolation ($\mu = 1$)

$$\begin{aligned} \hat{\phi}_1(\xi,\eta) &= \frac{1}{H^2}[\Phi_{ij}((i+1)H-\xi)((j+1)H-\eta) \\ &+ \Phi_{i+1\,j}(\xi - iH)((j+1)H-\eta) \\ &+ \Phi_{i\,j+1}((i+1)H-\xi)(\eta - jH) \\ &+ \Phi_{i+1\,j+1}(\xi - iH)(\eta - jH)] \quad \text{in } \tilde{\square}_{ij}, \end{aligned} \quad (2.7)$$

where

$$\begin{aligned} \tilde{\square}_{ij} &= \left\{ \begin{array}{ll} (\xi,\eta), & iH \leq \xi < (i+1)H, \\ & jH \leq \eta < (j+1)H \end{array} \right\}, \\ \textit{and} \ \ \Omega &= \bigcup_{ij} \tilde{\square}_{ij} \ . \end{aligned} \quad (2.8)$$

A pixel can be viewed as the representation of the mean greyness over $\square_{ij}$, given by

$$\Phi_{ij}^M = \frac{1}{H^2} \int\int_{\square_{ij}} \phi(\xi,\eta) d\xi d\eta \, . \quad (2.9)$$

Similarly, we have

$$B_{IJ}^M = \frac{1}{H^2} \int\int_{\square_{IJ}} b(x,y) dx dy, \quad (2.10)$$

where

$$\phi(\xi,\eta) = b(x(\xi,\eta), y(\xi,\eta)), \quad (2.11)$$

and the standard square pixel region

$$\square_{IJ} = \left\{ \begin{array}{ll} (x,y), & (I-\frac{1}{2})H \leq x < (I+\frac{1}{2})H \\ & (J-\frac{1}{2})H \leq y < (J+\frac{1}{2})H \end{array} \right\} \quad (2.12)$$

Note that the representation of image as the integrals in (2.9) and (2.10) is a key idea that enable us to develop new discrete algorithms by numerical approximation and to evaluate greyness errors by numerical analysis. The diagram of Figure 1 also illustrates our research process how to deal with discrete topics by continuous treatments and how to solicit numerical methods. We assume that the Jacobian determinants $\mathcal{J}(\xi,\eta)$ always satisfy

$$0 < \mathcal{J}_0 \le \mathcal{J}(\xi,\eta) \le \mathcal{J}_M\,, \tag{2.13}$$

where $\mathcal{J}_0$ and $\mathcal{J}_M$ are two bounded constants independent of ξ, η, x and y. For the inverse transformation T^{-1}, the integral (2.10) is reduced to

$$B_{IJ}^M = \frac{1}{H^2}\iint_{\Omega_{IJ}} \phi(\xi,\eta)\mathcal{J}(\xi,\eta)d\xi\,dy, \tag{2.14}$$

under

$$\square_{IJ} \xrightarrow{\mathrm{T}^{-1}} \Omega_{IJ},\ i.e.\ \ \Omega_{IJ} \xrightarrow{\mathrm{T}} \square_{IJ}. \tag{2.15}$$

Let the pixel region $\square_{ij}$ in $\xi o\eta$ of $\hat{W}_{ij}$ be split into N^2 small subregions $\square_{ij,k\ell}$, i.e., $\square_{ij} = \cup_{k,\ell=1}^{N} \square_{ij,k\ell}$, where

$$\square_{ij,k\ell} = \left\{ \begin{array}{ll} (\xi,\eta), & (i-\frac{1}{2})H + (k-1)h \le \\ & \xi < (i-\frac{1}{2})H + kh, \\ & (j-\frac{1}{2})H + (\ell-1)h \le \\ & \eta < (j-\frac{1}{2})H + \ell h \end{array} \right\}, \tag{2.16}$$

and h is the boundary length of $\square_{ij,k\ell}$, given by $h = \frac{H}{N}$. The splitting-shooting-method given in [5] collects the contribution of such subpixels $\square_{ij,k\ell}$ that whose transformed centroid by T falls into the identifying pixel region $\square_{IJ}$. As a result, we have

$$B_{IJ}^M = \frac{1}{H^2}\sum_{ij,k\ell}\iint_{\square_{ij,k\ell}\cap\Omega_{IJ}} \phi(\xi,\eta)\mathcal{J}(\xi,\eta)d\xi\,dy \tag{2.17}$$

Denote

$$\square_{ij,k\ell} \xrightarrow{\mathrm{T}} \square^*_{ij,k\ell}\,,\ \dot{G}_{ij,k\ell} \xrightarrow{\mathrm{T}} \dot{G}^*_{ij,k\ell}\,, \tag{2.18}$$

where $\dot{G}_{ij,k\ell}$ is the centroid of $\square_{ij,k\ell}$, we can see

$$\square_{ij,k\ell}\cap\Omega_{IJ} \xrightarrow{\mathrm{T}} \square^*_{ij,k\ell}\cap\square_{IJ}\,. \tag{2.19}$$

The following approximate integration can be obtained

$$\begin{aligned} B_{IJ}^M &\approx \tilde{B}_{IJ}^{(N)} \\ &= (\frac{h}{H})^2 \sum_{\forall(2.22)} \hat{\phi}_\mu(\dot{G}_{ij,k\ell})\,\mathcal{J}(\dot{G}_{ij,k\ell}),\ \mu = 0,1, \end{aligned} \tag{2.20}$$

where $\hat{\phi}_0$ and $\hat{\phi}_1$ are given in (2.5) and (2.7); and $\phi(\dot{G}) = \phi(\xi(\dot{G}),\eta(\dot{G}))$. The coordinates of $\dot{G} = \dot{G}_{ij,k\ell}$ are given by

$$\begin{aligned} \xi(\dot{G}) &= (i-\frac{1}{2})H + (k-\frac{1}{2})h, \\ \eta(\dot{G}) &= (j-\frac{1}{2})H + (\ell-\frac{1}{2})h\,. \end{aligned} \tag{2.21}$$

When the transformed centroid $\dot{G}^* = G^*_{ij,k\ell}$ falls into the standard square pixel region $\square_{IJ}$ defined in (2.12), the values of (I,J) can be computed by

$$I = \lfloor x(\dot{G}^*) + \frac{1}{2}\rfloor\,,\quad J = \lfloor y(\dot{G}^*) + \frac{1}{2}\rfloor\,, \tag{2.22}$$

where $\lfloor x\rfloor$ is the floor function, and

$$x(\dot{G}^*) = x(\xi(\dot{G}),\eta(\dot{G}))\,,\quad y(\dot{G}^*) = y(\xi(\dot{G}),\eta(\dot{G})) \tag{2.23}$$

Based on the greyness B_{IJ} obtained, we also construct the constant and bilinear functions $b_\mu(x,y)$ on the analogy of (2.5) and (2.7) , where $\hat{b}_0(x,y)$ in $\square_{IJ}$ and $\hat{b}_1(x,y)$ in $\tilde{\square}_{IJ}$ and

$$\tilde{\square}_{IJ} = \left\{ \begin{array}{ll} (x,y), & IH \le x < (I+1)H \\ & JH \le y < (J+1)H \end{array} \right\}. \tag{2.24}$$

The restored greyness (2.9) can be evaluated by the simplest centroid rule [1, 12].

$$\Phi_{ij} \approx \Phi_{ij}^M \approx \tilde{\phi}_{ij}^{(N)} = (\frac{h}{H})^2 \sum_{k,\ell=1}^{N} \hat{\phi}(\xi(\dot{G}),\eta(\dot{G}))\,, \tag{2.25}$$

where $\hat{\phi}(\xi,\eta) = \hat{b}_\mu(x,y)\,,\ \ \mu = 0,1.$

The evaluations (2.20) and (2.25) for pixel greyness are called the splitting-shooting method (SIM) and the splitting-integrating method (SIM) respectively. The combination of SSM and SIM is referred to CSIM, which will be discussed in the following two cases (see Figure 1). Case II consists of steps 1–8; Case I consists of Steps 1–4 and 6–8. In Case I, the greyness B_{IJ} after Step 3 will be used directly for T^{-1} without any changes. The distorted image $\{\hat{Z}\}$ may be obtained from $\{\tilde{B}_{IJ}\}$ in Step 4, but no feedback (i.e., from Z_{IJ} to B_{IJ} as in Step 5) is carried out.

3 Numerical Integration Using Partition Technique

We now intend to improve the integration approximations in (2.20) and (2.25) by using new partition techniques, to provide more accurate images. Denote

$$\square_{ij,k\ell} \xrightarrow{\mathrm{T}} \square^*_{ij,k\ell}. \tag{3.1}$$

A drawback of (2.20) is that all the contribution of the entire subpixel $\square_{ij,k\ell}$ with $\dot{G}^* \in \square_{IJ}$ is counted no matter how large a portion(e,g., even near a half) of $\square^*_{ij,k\ell}$ is located outside $\square_{IJ}$. Also the effect of $\square_{ij,k\ell}$ with $\dot{G}^* \notin \square_{IJ}$ is ignored even though $\square^*_{ij,k\ell}$ falls partially into $\square_{IJ}$. This drawback results in a low convergence rate $O(1/N)$ of image greyness under transformations. In order to obtain a better approximation of the integration, we have to distinguish carefully the parts of $\square^*_{ij,k\ell}$ that are located inside and outside the standard

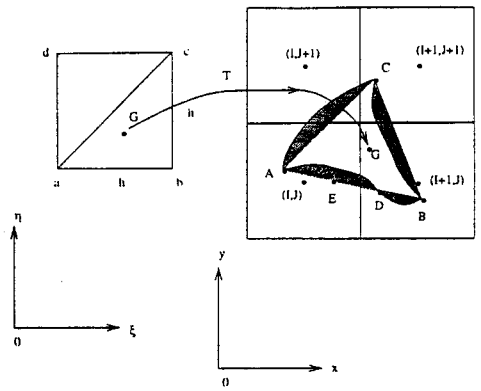

Figure 2: A transformation of a triangle $\triangle abc \xrightarrow{\mathrm{T}} \widehat{\triangle} ABC$

square pixel region $\square_{IJ}$, that is, to evaluate the overlaps of

$$\square^*_{ij,k\ell} \cap \square_{IJ} \text{ if } \square^*_{ij,k\ell} \cap \square_{IJ} \neq \emptyset\,. \tag{3.2}$$

There exist two different cases. **Case A.** The entire $\square^*_{ij,k\ell}$ falls into $\square_{IJ}$

$$\square^*_{ij,k\ell} \subseteq \square_{IJ}. \tag{3.3}$$

Case B. A part of $\square^*_{ij,k\ell}$ falls into $\square_{IJ}$

$$|\square^*_{ij,k\ell} \cap \square_{IJ}| < |\square^*_{ij,k\ell}|\,, \tag{3.4}$$

where $|\square|$ denotes the area of $\square$.

For Case A, the centroid rules is still employed for (2.17), to get

$$\begin{aligned}&\int\!\!\int_{\substack{\square_{ij,k\ell}\cap\Omega_{IJ}\\ Case\,A}} \tilde{\phi}(\xi,\eta)\mathcal{J}(\xi,\eta)d\xi\,d\eta\\ &= \int\!\!\int_{\square_{ij,k\ell}} \tilde{\phi}(\xi,\eta)\mathcal{J}(\xi,\eta)d\xi\,d\eta \approx h^2\tilde{\phi}_\mu(\dot{G})\mathcal{J}(\dot{G})\end{aligned} \tag{3.5}$$

For Case B, however, the following new refined technique is proposed. We have from (2.17) and (3.1)

$$\begin{aligned}&\int\!\!\int_{\substack{\square_{ij,k\ell}\cap\Omega_{IJ}\\ Case\,B}} \tilde{\phi}(\xi,\eta)\mathcal{J}(\xi,\eta)d\xi\,d\eta\\ &= \int\!\!\int_{\square^*_{ij,k\ell}\cap\square_{IJ}} \hat{b}(x,y)dx\,dy,\end{aligned} \tag{3.6}$$

where the portion (3.2) can be carefully evaluated through three steps described below. **Step I.** *Choice of* N to simplify the partition situation. We choose N so that any $\square^*_{ij,k\ell}$ is located, at most within the following four pixel regions:

$$\square^*_{ij,k\ell} \leq (\square_{IJ} \cup \square_{I+1\,J} \cup \square_{I\,J+1} \cup \square_{I+1\,J+1})\,. \tag{3.7}$$

Step II. *Partitions of Squares.* Divide a subregion, $\square_{ij,k\ell}$ in $\xi o\eta$ by a diagonal into two triangular elements (see Figure 2)

$$\square_{ij,k\ell} = \bigcup_{t=1,2} \triangle_{ij,k\ell,t}. \tag{3.8}$$

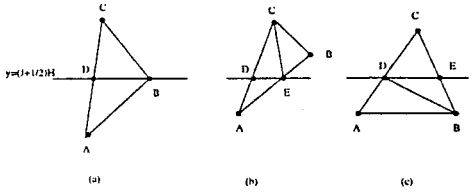

Figure 3: Three cases of dividing $\triangle ABC$ by the horizontal line $y = (J + \frac{1}{2})H$

Denote

$$\triangle_{ij,k\ell,t} \xrightarrow{\mathrm{T}} \widehat{\triangle}^*_{ij,k\ell,t} \approx \hat{\triangle}^*_{ij,k\ell,t}. \tag{3.9}$$

which is also represented as in Figure 2 by

$$\triangle abc \xrightarrow{\mathrm{T}} \widehat{\triangle}\, ABC \approx \hat{\triangle} ABC\,, \tag{3.10}$$

with $a \xrightarrow{\mathrm{T}} A$, $\overline{ab} \xrightarrow{\mathrm{T}} \widehat{AB}$, etc. where $\widehat{\triangle}^*_{ij,k\ell,t}$ in xoy has three vertices A, B and C, and three curved boundaries under the relations(see Figure 2): Consequently, the overlaps (3.2) lead to

$$\square^*_{ij,k\ell} \cap \square_{IJ} \approx \bigcup_{t=1,2} (\hat{\triangle}^*_{ij,k\ell,t} \cap \square_{IJ})\,. \tag{3.11}$$

Step III. *Partitions of triangles.* Based on the chosen N in Step I, for any $\hat{\triangle}^*_{ij,k\ell,t}$ there exists, at most, one boundary line of

$$x = (I \pm \frac{1}{2})H\,, \qquad y = (J \pm \frac{1}{2})H\,, \tag{3.12}$$

along x or y that can pass through its middle. Moreover, let A,B, and C denote the top, middle, and bottom vertices of $\triangle ABC$. For instance, we partition $\triangle ABC$ by a horizontal boundary line,

$$y = \overline{y} = (J + \frac{1}{2})H \tag{3.13}$$

such that

$$\triangle ABC \cap (y \geq \overline{y}) \text{ or } \triangle ABC \cap (y \leq \overline{y})\,. \tag{3.14}$$

For simplicity, we may partition $\triangle ABC$ into sub-triangles such a way that each sub-triangle is located either above or under the boundary line (3.13). The following three situations will occur that lead to different partitions of triangles, due to different locations of the boundary line (3.13) as illustrated in Figure 3. **I.** When the middle vertex B is just on line (3.13), we may split $\triangle ABC$ into two triangles,

$$\triangle ABC = \triangle^+ ABD \cup \triangle^- BCD, \tag{3.15}$$

where $\triangle^+$ and $\triangle^-$ denote the upper triangle and the lower triangle respectively, with respect to (3.13). **II.** When line (3.13) is located between the vertices A and B, $\triangle ABC$ is split into three triangles:

$$\triangle ABC = \triangle^- AED \cup \triangle^+ DEC \cup \triangle^+ EBC, \tag{3.16}$$

where E is the intersection point of $\overline{AB}$ and line (3.13), with the coordinates,

$$y_E = \overline{y}\,, \quad x_E = x_A + \frac{\overline{y} - y_A}{y_B - y_A}(x_B - x_A)\,. \quad (3.17)$$

III. When line (3.13) is located between the vertices B and C, then

$$\triangle ABC = \triangle^{-}ABD \cup \triangle^{-}BDE \cup \triangle^{+}DEC. \quad (3.18)$$

By (3.15), (3.16) and (3.18), we split $\triangle ABC$ into the sub-triangles which are no longer traversed by the horizontal boundary line (3.13). Furthermore, some of these sub-triangles may still be traversed by a vertical boundary coordinate lines

$$x = \overline{x} = (I + \frac{1}{2})H. \quad (3.19)$$

By means of the same technique as in Steps I–III, we can split such a sub-triangle into smaller sub-triangles again so that none of the sub-triangles is crossed by all the boundary lines, (3.12), of $\square_{IJ}$. Let us summarize the partition of triangle $\hat{\triangle}^{*}_{ij,k\ell,t}$ by Steps I–III. If regarding $\hat{\triangle}^{*}_{ij,k\ell,t}$ as $\triangle ABC$ in xoy in Figure 3, we obtain

$$\hat{\triangle}^{*}_{ij,k\ell,t} = \bigcup_{m} \hat{\triangle}^{*}_{ij,k\ell,t,m}, \quad m \le 9, \quad (3.20)$$

where all the sub-triangles will fall into just one of the following pixel regions.

$$\hat{\triangle}^{*}_{ij,k\ell,t,m} \subseteq \square_{I+I_0,J+J_0}\,, \quad I_0, J_0 = 0 \text{ or } 1. \quad (3.21)$$

Applying the above technique, we can improve evaluation of integration. First we have from (2.17), (3.5) and (3.6)

$$\begin{aligned} B^{M}_{IJ} &= \frac{1}{H^2}\sum_{ij,k\ell}\int\!\!\int_{\square_{ij,k\ell}\cap\Omega_{IJ}} \phi(\xi,\eta)\mathcal{J}(\xi,\eta)d\xi\,d\eta \\ &\approx (\frac{h}{H})^2 \sum_{\substack{ij,k\ell \\ Case\,A}} \phi(\dot{G})\mathcal{J}(\dot{G}) \quad (3.22) \\ &+ \frac{1}{H^2}\sum_{\substack{ij,k\ell \\ Case\,B}} \int\!\!\int_{\square_{ij,k\ell}\cap\Omega_{IJ}} \phi(\xi,\eta)\mathcal{J}(\xi,\eta)d\xi\,d\eta\,. \end{aligned}$$

Next, we obtain from (3.6) and (3.20) for Case B,

$$\begin{aligned} &\int\!\!\int_{\square_{ij,k\ell}\cap\Omega_{IJ}} \phi(\xi,\eta)\mathcal{J}(\xi,\eta)d\xi\,d\eta \\ &= \int\!\!\int_{\square^{*}_{ij,k\ell}\cap\square_{IJ}} b(x,y)dx\,dy \\ &= \sum_{t=1}^{2}\int\!\!\int_{\hat{\triangle}^{*}_{ij,k\ell,t}\cap\square_{IJ}} \hat{b}(x,y)dx\,dy \\ &\approx \sum_{t,m}\int\!\!\int_{\hat{\triangle}^{*}_{ij,k\ell,t,m}} \hat{b}(x,y)dx\,dy \\ &\approx b(\dot{G}^{*}) \sum_{\substack{t,m \\ \forall(3.24)}} |\hat{\triangle}^{*}_{ij,k\ell,t,m}|, \quad (3.23) \end{aligned}$$

where $\dot{G}^{*}$ denotes the center of gravity of $\hat{\triangle}^{*}_{ij,k\ell,t,m}$ in xoy, satisfying

$$\hat{\triangle}^{*}_{ij,k\ell,t,m} \subseteq \square_{IJ} \quad (3.24)$$

The area of a triangle in (3.23) can be computed by the formula (see [9]). Consequently, the renovated splitting-shooting method (called $\overline{\mathrm{S}}\,\overline{\mathrm{S}}\mathrm{M}$) using the partition technique from (3.22) and (3.23) yields greyness B_{IJ} under T by

$$\begin{aligned} B_{IJ} \approx \overset{\approx}{B}{}^{(N)}_{IJ} &= (\frac{h}{H})^2 \sum_{\substack{ij,k\ell \\ Case\,A}} \hat{\phi}(\dot{G})\mathcal{J}(\dot{G}) \\ &+ \frac{1}{H^2}\sum_{\substack{ij,k\ell \\ Case\,B}} \hat{b}(\dot{G}^{*}) \sum_{\substack{t,m \\ \forall(3.24)}} |\hat{\triangle}^{*}_{ij,k\ell,t,m}|\,. \quad (3.25) \end{aligned}$$

As to the splitting-integrating method (SIM) for T^{-1} , the convergence rates of pixel greyness solutions can reach $O(1/N^2)$ only when $\mu = 1$. When using the piecewise constant interpolation ($\mu = 0$), the low convergence rate $O(1/N)$ still occurs. Therefore in this case, the partition technique should also be adopted to modify SIM as well. In fact, the greyness (2.9) leads to

$$\begin{aligned} \Phi^{M}_{ij} &\approx \frac{1}{H^2}\sum_{\substack{k,\ell \\ Case\,A}} \int\!\!\int_{\square_{ij,k\ell}} \hat{\phi}(\xi,\eta)d\xi\,d\eta \\ &+ \frac{1}{H^2}\sum_{\substack{k,\ell \\ Case\,B}} \int\!\!\int_{\square_{ij,k\ell}\cap\Omega_{IJ}} \hat{\phi}(\xi,\eta)d\xi\,d\eta\,. \quad (3.26) \end{aligned}$$

For Case A, the centroid rule is also valid, yielding

$$\int\!\!\int_{\substack{\square_{ij,k\ell} \\ Case\,A}} \hat{\phi}(\xi,\eta)d\xi\,d\eta \approx h^2\hat{\phi}(\dot{G})\,. \quad (3.27)$$

On the other hand, for Case B as $\mu = 0$, we have from (3.8) and (3.20)

$$\begin{aligned} &\int\!\!\int_{\square_{ij,k\ell}\cap\Omega_{IJ}} \hat{\phi}(\xi,\eta)d\xi\,d\eta \\ &= \int\!\!\int_{\square^{*}_{ij,k\ell}\cap\square_{IJ}} \hat{b}_0(x,y)\mathcal{J}^{-1}dx\,dy \\ &\approx \sum_{\substack{t,m \\ \forall(3.24)}} B_{IJ}\int\!\!\int_{\hat{\triangle}^{*}_{ij,k\ell,t,m}} \mathcal{J}^{-1}dx\,dy\,, \end{aligned}$$

where $\mathcal{J}$ is the Jacobian determinant. Since

$$\frac{1}{J} \approx \frac{|\hat{\triangle}_{ij,k\ell,t}|}{|\hat{\triangle}^{*}_{ij,k\ell,t}|} = \frac{h^2}{2}\,/\,|\hat{\triangle}^{*}_{ij,k\ell,t}|\,, \quad (3.28)$$

we have

$$\int\!\!\int_{\hat{\triangle}^{*}_{ij,k\ell,t,m}} \mathcal{J}^{-1}dx\,dy \approx \frac{h^2}{2}\,\frac{|\hat{\triangle}^{*}_{ij,k\ell,t,m}|}{|\hat{\triangle}^{*}_{ij,k\ell,t}|}\,. \quad (3.29)$$

Consequently, from (3.26)–(3.29) the splitting-integrating method ($\overline{\mathrm{S}}\,\overline{\mathrm{I}}\mathrm{M}$) using the partition

technique seeks image greyness under T^{-1} when $\mu = 0$, by

$$\Phi_{ij} \approx \tilde{\Phi}_{ij}^{(N)} = \sum_{\substack{k,\ell \\ Case A}} (\frac{h}{H})^2 \hat{\phi}(\dot{G}) + \sum_{\substack{k,\ell \\ Case B}} \sum_{\substack{t,m \\ \forall(3.24)}} \frac{1}{2}(\frac{h}{H})^2 B_{IJ} \frac{|\hat{\Delta}^*_{ij,k\ell,t,m}|}{|\hat{\Delta}^*_{ij,k\ell,t}|}. \quad (3.30)$$

Combining (3.25) and (2.20) leads to CS̄IM, and combining (3.25) and (3.30) leads to CS̄ĪM as $\mu = 0$. Note that both CS̄IM and CS̄ĪM do not require solutions of nonlinear equations either.

4 Error Bounds of Integration Approximation and image Greyness

It is clear that the discrete algorithms in Section 3 are of numerical integration, basically. However, the integration approximations, (3.25), and (3.30), are not the same as the traditional methods in [1, 12]. Such a distinctness results from different regularities of the integrand in different subregions due to *piecewise* bilinear interpolation. Therefore, error analysis on new algorithms is necessary and important. We will define some error norms to measure the approximation degree of greyness solutions. Choose the division number

$$N = N_p = 2^p, \ \textit{where } p = p_0,\ p_0 + 1,\ \textit{integer } p_0 > 0. \quad (4.1)$$

Define the consecutive errors of image greyness under T^{-1} or $T^{-1}T$ with the two division numbers N_p and N_{p-1}:

$$\Delta E^{(N_p)}(\tilde{\Phi}) = \sum_{ij} \frac{|\tilde{\Phi}_{ij}^{(N_p)} - \tilde{\Phi}_{ij}^{(N_{p-1})}|}{I_{\max}(\tilde{W})},$$

$$\Delta E_2^{(N_p)}(\tilde{\Phi}) = \{ \sum_{ij} \frac{(\tilde{\Phi}_{ij}^{(N_p)} - \tilde{\Phi}_{ij}^{(N_{p-1})})^2}{I_{\max}(\tilde{W})} \}^{1/2}, \quad (4.2)$$

where $I_{\max}(\tilde{W})$ is the total number of nonempty pixels, defined by

$$I_{\max}(\tilde{W}) = \sum_{ij} N_f(\tilde{W}_{ij}^{(N_p)}),$$

$$N_f(W_{ij}) = \begin{cases} 1 & \text{if } W_{ij} \neq \text{`\ '}, \\ 0 & \text{if } W_{ij} = \text{`\ '}. \end{cases} \quad (4.3)$$

The details of analysis can be found in [13]; we only give an important corollary.

Corollary 4.1 *Let (4.1) and all conditions in Theorems 4.1 - 4.3 in [13] ahold true; also assume* $\phi(\xi, \eta) \in C^2(\Omega)$. *Then when* $N \to \infty$, *the image greyness under* $T^{-1}T$ *by* $C\bar{S}IM$ *in Case I has the asymptotic relations*

$$E(\tilde{\Phi}^*) = O(\frac{1}{H^2}) + O(1/N^{\mu+1}),$$
$$\Delta E(\tilde{\Phi}^*) = O(1/N^{\mu+1}), \quad \mu = 0, 1. \quad (4.4)$$

Also when $\mu = 0$ *and* $N \to \infty$, *the image greyness under* $T^{-1}T$ *by* $C\bar{S}\bar{I}M$ *as* $\mu = 0$ *in Case I has the asymptotic relations*

$$E(\tilde{\tilde{\Phi}}^*) = O(\frac{1}{H^2}) + O(1/N^2),$$
$$\Delta E(\tilde{\tilde{\Phi}}^*) = O(1/N^2). \quad (4.5)$$

The new combinations CS̄IM as $\mu = 1$ and CS̄ĪM as $\mu = 0$ can produce the images under $\mathrm{T}^{-1}\mathrm{T}$ with the better convergence rate $O(1/N^2)$.

5 Numerical and Graphical Experiments

We may also define the pixel error under $T^{-1}T$

$$\Delta I_\ell^{(N_p)}(\tilde{W}) = \sum_{ij} N_{d,\ell}(\tilde{W}_{ij}^{(N_p)} - \tilde{W}_{ij}^{(N_{p-1})}),$$
$$I_\ell^{(N_p)}(\tilde{W}) = \sum_{ij} N_{d,\ell}(\tilde{W}_{ij}^{(N_p)} - W_{ij}),$$

where

$$N_{d,\ell}(W_1 - W_2) = \begin{cases} 1 & if\ (W_1 \neq W_2) \wedge \\ & ((W_1 = G_\ell) \vee (W_2 = G_\ell)), \\ 0 & \text{otherwise}, \end{cases} \quad (5.1)$$

and $G_1 = \text{`}*\text{'}$, $G_2 = \text{`}+\text{'}$, $G_3 = \text{`}\cdot\text{'}$ Let the standard image W be given in Figure 4, and T be a bi-quadratic transformation in [6]. The pixel greyness under $T^{-1}T$ is evaluated by CS̄IM and CS̄ĪM. Their error curves of ΔE are depicted in Figures 5 and 6. It can be seen that

$$\Delta E^{(N)}(\tilde{\tilde{B}}) = O(1/N^2)$$
$$by\ \bar{S}\bar{S}M\ as\ \mu = 0, 1; \quad (5.2)$$

$$\Delta E^{(N)}(\tilde{\Phi}^*) = O(1/N^{\mu+1}),$$
$$by\ C\bar{S}IM\ as\ \mu = 0, 1.\ in\ Case\ I; \quad (5.3)$$

$$\Delta E^{(N)}(\tilde{\tilde{\Phi}}^*) = O(1/N^2),$$
$$by\ C\bar{S}\bar{I}M\ as\ \mu = 0\ in\ Case\ I. \quad (5.4)$$

All the experimental results (5.2)–(5.4) confirm the analysis in Section 4. We provide some images under transformation by CS̄IM and CS̄ĪM in Figures 7 - 8. Furthermore, Figure 8 indicates that Combination CS̄ĪM is also well suited to the transformation

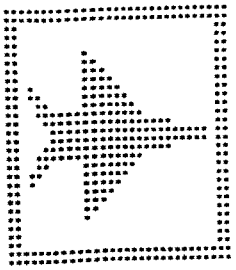

Figure 4: A standard image

of curve images, which often cause troubles by many other approaches. Next, consider the different division numbers N_{ford} and N_{back} used for T and T^{-1} in C$\bar{S}$IM respectively. We choose $N_{ford} = 8$ in $\bar{S}\,\bar{S}$M; and $N_{back} = 1, 2, 4, \cdots, 32$ in SIM. Denote $S(N_{ford}, N_{back})$ as the greyness solution using N_{ford} for T and N_{back} for T^{-1}. We list in Table 3 in [13] the errors between $S(32, 32)$ and $S(8, N_{back})$ and the absolute errors between $S(8, N_{back})$ and the true solutions. Table 3 in [13] indicates the optimal division number is about $N_{back} = 8$. We then conclude that an equal number, $N_{back} = N_{ford} = N$, is a good choice. As a consequence, we always choose the same division number for both T and T^{-1} in CSIM and their renovation. We collect in Table 4 in [13] all the errors by different combinations CSIM, C$\bar{S}$IM and C$\bar{S}\,\bar{I}$M when $N = 8$. The absolute errors E obtained from both C$\bar{S}$IM (as $\mu = 1$) and C$\bar{S}\,\bar{I}$M (as $\mu = 0$) are significantly smaller than those obtained from CSIM (as $\mu = 0, 1$) cited from [7]. For example, the ratios of restoring greyness errors under $T^{-1}T$ are

$$\frac{\Delta E|_{\text{CSIM}}}{\Delta E|_{\text{C}\bar{\text{S}}\text{IM}}} = \frac{0.04054}{0.001973} = 20.55 \text{ as } \mu = 1, \qquad (5.5)$$

$$\frac{\Delta E|_{\text{CSIM}}}{\Delta E|_{\text{C}\bar{\text{S}}\,\bar{\text{I}}\text{M}}} = \frac{0.06865}{0.1180 * 10^{-3}} = 581.8 \text{ as } \mu = 0. \qquad (5.6)$$

This clearly displays a significant advantage of C$\bar{S}$IM and C$\bar{S}\,\bar{I}$M over CSIM in [5, 8]. The above examples are all binary images; we now apply C$\bar{S}$IM and C$\bar{S}\,\bar{I}$M to real images of 256 × 256 pixels with 256 grayness levels. Choosing $N = 4$, the computer images are produced under transformations, and illustrated in Figures 9-11. The original and restored girl-images are shown on the left and right sides of the top in the figures respectively. For Figure 9 using C$\bar{S}$IM the distorted image has about 124000 nonempty pixels. Compared with the images by C$\bar{S}$IM as $N = 8$, the average levels of sequential errors are only 0.02, which are very small, indeed, in 256 levels counted. As to the restored image of Figure 9, the sequential and absolute pixel errors are only 0.03 and 4.3 respectively. For Figure 10 using C$\bar{S}\,\bar{I}$M as $\mu = 0$, the distorted image has 0.08 greyness levels of sequential errors; and the restored image has 0.03 and 9.1 greyness levels of sequential and absolute errors, respectively.

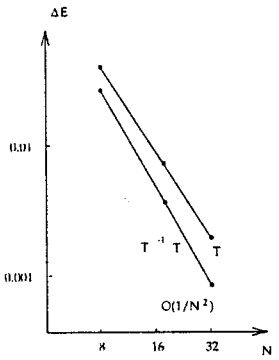

Figure 5: Error curves of ΔE versus N by C$\bar{S}$IM in Case I as $\mu = 1$

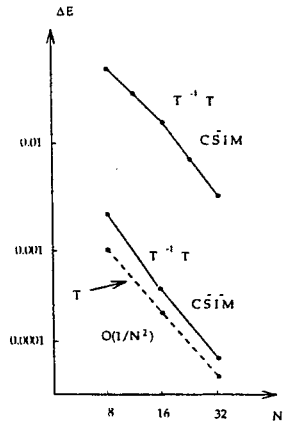

Figure 6: Error curves of ΔE versus N by C$\bar{S}$IM and C$\bar{S}\,\bar{I}$M in Case I as $\mu = 0$

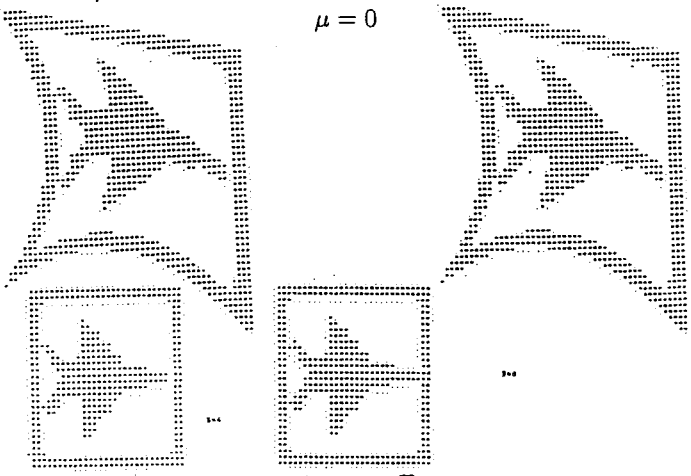

Figure 7: Images under $T^{-1}T$ by C$\bar{S}$IM in Case I as $\mu = 1$, a) as N=4, b) as N=8.

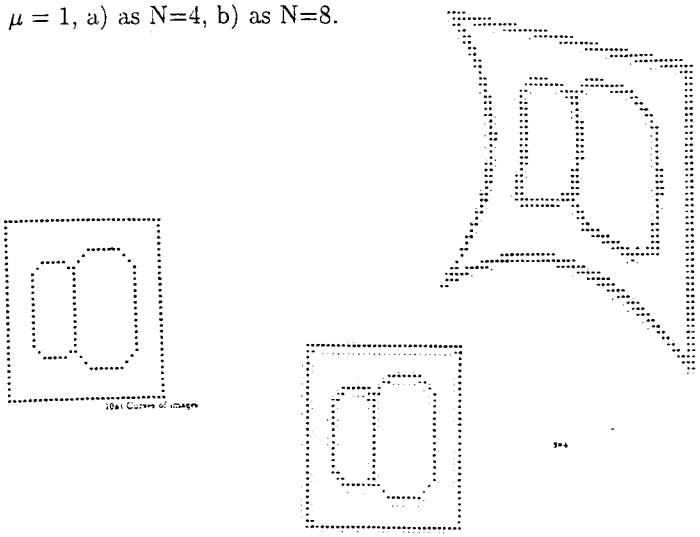

Figure 8: (a) Curves of images (b) Images of curves under $T^{-1}T$ by C$\bar{S}\,\bar{I}$M in Case I as $N = 4$ and $\mu = 0$.

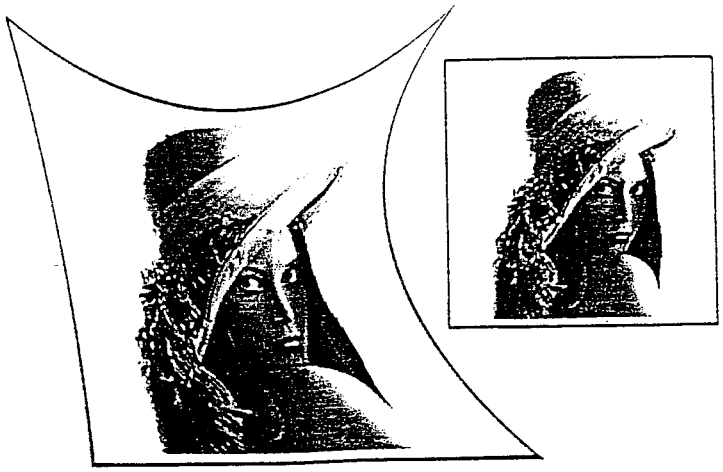

Figure 9: The girl-images of 256 × 256 pixels with 256 greyness levels under $T^{-1}T$ by CSIM in Case I as $\mu = 1$ and $N = 4$.

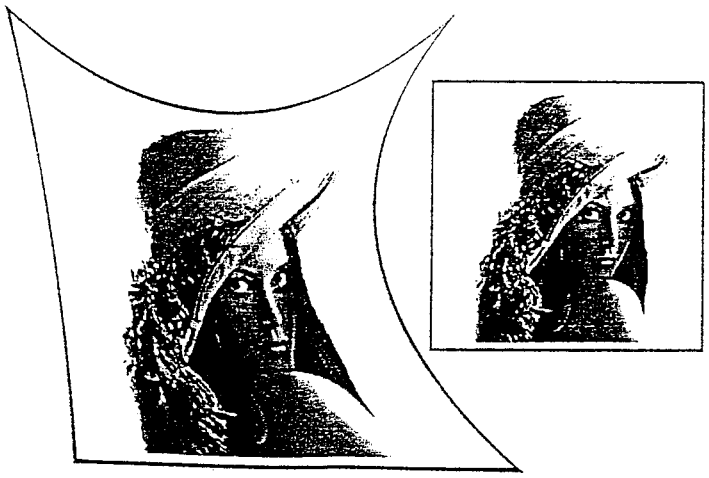

Figure 10: The girl-images of 256 × 256 pixels with 256 greyness levels under $T^{-1}T$ by CSIM in Case I as $\mu = 0$ and $N = 4$.

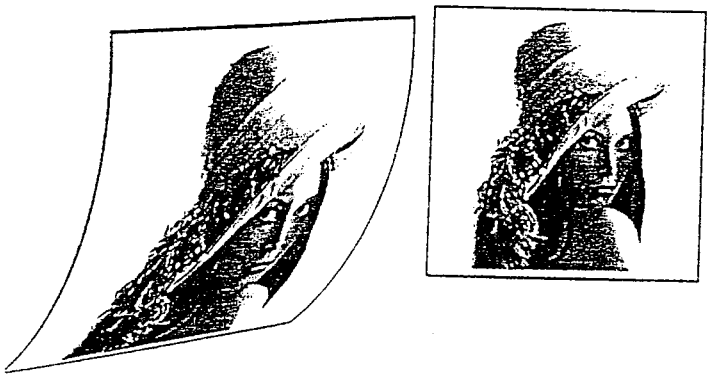

Figure 11: The girl-images of 256 × 256 pixels with 256 greyness levels under $T^{-1}T$ by CSIM in Case I as $\mu = 0$ and $N = 4$ for the perspective transformation.

References

[1] P.J. Davis and P. Rabinowitz, **Method of Numerical Integration**, 2nd Edition, Academic Press Inc., 1984.

[2] E. R. Dougherty and C. R. Giardina, **Image Processing-Continuous to Discrete, Vol I., Geometric, Transform and Statistical Methods** , Prentice-Hall, Inc., Englewood Cliffs, 1987.

[3] J.D. Foley, A. van Dam, S.K. Feiner and J.K. Hughes, **Computer Graphics, Principles and Practice**, 2nd Edition, Addison-Wesley, 1990.

[4] R.C. Gouzaler and P. Winter, **Digital Image Processing**, 2nd Edition, Addison-Wesley, 1977.

[5] Z.C. Li, Discrete techniques for computer transformations of digital images and patterns, *Pattern Recognition*, vol. 23, pp.1249–1273, 1990.

[6] Z.C. Li, Splitting-integrating method for inverse transformation of n-dimensional digital images and patterns, Numerical Algorithms, vol.9, p.181-198, 1995.

[7] Z.C. Li, Analysis on discrete techniques for computer transformations of digital images and patterns, Numerical Algorithms, vol.13, p.225-263, 1996.

[8] Z.C. Li and Z.D.Bai, Probabilistic analysis on the splitting-shooting method for image transformations to appear in J. Comp. and Appl. Math, 1998.

[9] Z.C. Li, T.D. Bui, Y.Y. Tang and C.Y. Suen, **Computer Transformation of Digital Images and Patterns**, World Scientific Publishing, 1989.

[10] W.K.Pratt, **Digital Image Processing**(Sec. Ed.), John Wiley & Sons Inc., 1991.

[11] D.F.Rogers and J. A. Adames, **Mathematical Elements for Computer Graphics**(Sec. Ed.), McGraw-Hill Pub. Company, 1990.

[12] A.H. Stroud, **Approximate Calculation of Multiple Integrals**, Prentice-Hall Inc., 1971.

[13] Z.C. Li, Advanced Combinations of Splitting-Shooting-Integrating Methods for Digital Image Transformations